



Journal Name

ARTICLE

## A facile way to prepare nanoporous $\text{PbI}_2$ films and their application in fast conversion into $\text{CH}_3\text{NH}_3\text{PbI}_3$ †

Huifeng Zheng,<sup>a</sup> Weiqi Wang,<sup>a</sup> Songwang Yang,<sup>b</sup> Yangqiao Liu,<sup>\*a</sup> and Jing Sun<sup>\*a</sup>Received 00th January 20xx,  
Accepted 00th January 20xx

DOI: 10.1039/x0xx00000x

[www.rsc.org/](http://www.rsc.org/)

In this report, we demonstrate a facile way to prepare  $\text{PbI}_2$  films with interpenetrating nanopores. The nanoporous  $\text{PbI}_2$  (n- $\text{PbI}_2$ ) films were prepared by the solvent-solvent extraction (SSE) method, in which the DMF solvent was effectively extracted by isopropanol (IPA) within seconds, resulting in well-crystallized n- $\text{PbI}_2$  films without annealing. The mechanism involved in preparation of n- $\text{PbI}_2$  films using the SSE method was studied further, and some universal rules of fabricating n- $\text{PbI}_2$  films with the SSE method were proposed. The interpenetrating nanoporous morphology enabled the fast penetration of  $\text{CH}_3\text{NH}_3\text{I}$  (MAI) solution, so most part of  $\text{PbI}_2$  converted into  $\text{CH}_3\text{NH}_3\text{PbI}_3$  within 10 s even with a perovskite overlayer of 300 nm. Moreover, the perovskite layer was pinhole-free and smoother than that based on conventional  $\text{PbI}_2$  film. Consequently, perovskite solar cells based on n- $\text{PbI}_2$ , with setup as FTO/Compact  $\text{TiO}_2$ /Bilayer  $\text{CH}_3\text{NH}_3\text{PbI}_3$ /P3HT/Ag, delivered a champion power conversion efficiency of 10.1%, compared with 5.9% for its counterpart based on conventional compact  $\text{PbI}_2$  film. This work unveils the  $\text{PbI}_2$ -morphology-related reaction kinetics in the two-step method, and will contribute to understanding the role of  $\text{PbI}_2$  films playing in the preparation of perovskite.

### Introduction

Organometal halide perovskites have been a hot topic in the field of solar cells, due to its excellent properties such as a high extinction coefficient,<sup>1</sup> long carrier diffusion length<sup>2-4</sup> and a tunable bandgap<sup>5-9</sup>. Recently, its power conversion efficiency has reached over 20%.<sup>10</sup> Perovskite films are usually prepared in three methods: (1) one-step solution deposition;<sup>11,12</sup> (2) two-step solution deposition;<sup>13</sup> (3) vapor deposition.<sup>14,15</sup> Generally, the two-step method offers better control of the films' morphology than the one-step method,<sup>16,17</sup> and is much cheaper, more convenient than the vapor deposition.

The critical step in the two-step method is dipping  $\text{PbI}_2$  films into  $\text{CH}_3\text{NH}_3\text{I}$  (MAI) solution to react. However, the reaction takes tens of minutes to 2 hours, for planar structure<sup>13,18</sup> or bilayer structure<sup>19,20</sup> comprising mesoscopic and planar layers.<sup>21-23</sup> However, dipping too long results in: (1) the abnormal growth of perovskite crystals;<sup>23,24</sup> (2) the dissolution or peel-off of perovskite films,<sup>18,25</sup> both of which will deteriorate the efficiency. To shorten the dipping time, isopropanol (IPA) pre-wetting<sup>13,26</sup> and increasing reaction

temperature<sup>26-28</sup> are common practices. However, both of them accelerates the reaction between  $\text{PbI}_2$  and  $\text{CH}_3\text{NH}_3\text{I}$  as well as the abnormal growth of perovskite crystals,<sup>26</sup> detrimental to the reproducibility.<sup>27</sup> So, it is in great demand for a facile method to accelerate the reaction without causing the abnormal growth of perovskite crystals for planar and bilayer structure.

Recently, some researchers proposed the application of porous  $\text{PbI}_2$  films to facilitate the reaction.<sup>29,30</sup> As the reaction between  $\text{PbI}_2$  (solid) and MAI (in IPA) is essentially a solid-liquid reaction, the larger specific area is the more reaction sites there are, promising a higher reaction rate.<sup>25</sup>

However, in those reports the porous  $\text{PbI}_2$  films consisting of nano-sheet arrays were fabricated by vacuum thermal evaporation, which was too complex for preparation and not energy-saving.<sup>29,30</sup> Furthermore, porous  $\text{PbI}_2$  was attainable only when polycrystalline substrates were applied.<sup>29</sup> Besides, Zhou *et al.* prepared nanoporous  $\text{PbI}_2$  (n- $\text{PbI}_2$ ) by air blowing and drying at room temperature.<sup>31</sup> Whereas, this method takes several hours to prepare, due to the low volatility of the solvent (dimethyl formamide, DMF) at room temperature. Here, we demonstrate a facile way to synthesize  $\text{PbI}_2$  films with interpenetrating nanopores by the solvent-solvent extraction (SSE) method.<sup>32</sup> The SSE is a process in which solute crystallized as a result of extracting the main solvent by another poor solvent. The SSE process was first reported in the fabrication of perovskite layers with the one-step method, but never reported in preparing nanoporous  $\text{PbI}_2$  films. Using this method, it only takes less than 1 min to prepare well-crystallized nanoporous  $\text{PbI}_2$  films without annealing. As

<sup>a</sup> State Key Laboratory of High Performance Ceramics and Superfine Microstructure, Shanghai Institute of Ceramics, Chinese Academy of Sciences, 1295 Dingxi Road, Shanghai 200050, P. R. China.  
E-mail: yqliu@mail.sic.ac.cn, jingsun@mail.sic.ac.cn

<sup>b</sup> CAS Key Laboratory of Materials for Energy Conversion, Shanghai Institute of Ceramics, Chinese Academy of Sciences, 588 Heshuo Road, Shanghai 201899, P. R. China

†Electronic Supplementary Information (ESI) available. See DOI: 10.1039/x0xx00000x

expected, the resultant n-PbI<sub>2</sub> films significantly accelerate the reaction rate. Most part of PbI<sub>2</sub> in n-PbI<sub>2</sub> films converted into perovskite within 10 s, in stark contrast to the 10 min which was needed for conventional compact PbI<sub>2</sub> films. By dipping for 40 s, we obtained pinhole-free bilayer-structured perovskite films with 300 nm overlayer, resulting in the champion efficiency above 10%.

## Experimental

### Materials

In the fabrication of perovskite and hole transporting layers, all solvents involved were dehydrated by molecular sieves (4A), such as dimethyl formamide (DMF), isopropanol (IPA), toluene. All other materials were used as received.

CH<sub>3</sub>NH<sub>3</sub>I was prepared according to literature.<sup>15</sup> Specifically, 50 ml methylamine (33 wt%, in absolute ethanol, Aldrich) and 20 ml hydriodic acid (57 wt% in water, J&k Scientific) were reacted in a 500 ml round-bottom flask in the ice bath with stirring under N<sub>2</sub> for 2 h. After that, the solution was evaporated at 50 °C for 1 h to obtain yellowish precipitate, which was washed with diethyl ether twice. Finally, the solid was dried at 60 °C in vacuum for 24 h.

### Fabrication of perovskite solar cells

Fluorine-doped tin oxide (FTO; 15 Ω/□, Nippon Sheet Glass) glass substrates were patterned by Zn powder and HCl (concentrated HCl:H<sub>2</sub>O=2:3 by volume) for 90 s. The resultant FTO substrates were cleaned sequentially in detergent (Hellmanex II, 2%), water, ethanol, acetone, ethanol with ultrasonication for 30 min and then treated with ultraviolet (UV) for 15 min. A 30 nm thick TiO<sub>2</sub> compact layer was then deposited by spin coating at 6000 r.p.m for 30 s with a weakly acidic solution of titanium isopropoxide (Aldrich) reported by Snaith's group.<sup>33</sup> After drying at 70 °C, the films were annealed at 500 °C for 30 min. Then, the films were treated in 40 mM TiCl<sub>4</sub> aqueous solution for 30 min at 70 °C, rinsed with deionized water and ethanol and dried at 500 °C for 30 min.

The mesoporous TiO<sub>2</sub> was prepared with reported method.<sup>13</sup> After drying at 70 °C, the TiO<sub>2</sub> films were sintered at 500 °C for 30 min. Then, the resultant films were treated with 40 mM TiCl<sub>4</sub> for another 30 min, followed by being annealed at 500 °C for 30 min. The mesoporous TiO<sub>2</sub> films were filled by spin coating of 1M PbI<sub>2</sub> (Sigma) in DMF at 4000 r.p.m with (for preparing n-PbI<sub>2</sub> films) or without (for preparing c-PbI<sub>2</sub> films) SSE post-treatment. The SSE process was that 100 μl IPA solution was dispensed on the surface of pristine PbI<sub>2</sub> films (without annealing) for several seconds, then spin at 4000 r.p.m for 60 s. The resultant PbI<sub>2</sub> films were dried at 75 °C for 30 min, before cooling down to room temperature. For preparation of perovskite films, the PbI<sub>2</sub> films were dipped into 10 mg/ml MAI in IPA for tens of seconds, which was kept at 50 °C. After being rinsed with IPA, the perovskite films were dried at 75 °C for 30 min. When those substrates cold down, a solution of poly-3-hexylthiophene (P3HT: J&k Scientific, RMI-

001EE) was spin-coated, whose composition was: P3HT/toluene 15 mg/mL, 7.5 μL Li-bis(trifluoromethanesulfonyl)imide (Li-TFSI, Aldrich)/acetonitrile (170 mg/1 mL) and 7.5 μL 4-tert-Butylpyridine (t-BP, Aldrich)/acetonitrile (1 mL/1 mL).<sup>34</sup> All these steps involving perovskite films and P3HT layer were conducted inside an Ar-filled glovebox. Finally, ~80 nm Ag was thermally evaporated through a shadow mask under vacuum (ca.3x10<sup>-3</sup>Pa). The effective area for device was 0.15 cm<sup>2</sup>.

### Characterization

X-ray diffraction (XRD) spectra were obtained from Rigaku D/max 2550V with Cu Kα radiation at a step size of 0.02°. The absorption spectra of perovskite films were characterized by a UV/Vis/NIR spectrophotometer (Lambda 950, Perkin Elmer). The composition of chemical bonding was measured by Fourier Transform Infrared Spectroscopy (FTIR) with Bruker, Tensor 27 using the standard Pike ATR cell. The morphology of perovskite films was observed by scanning electron microscopy (SEM; SU8220, Hitachi, Japan). PbI<sub>2</sub> nanoparticles, scratched from PbI<sub>2</sub> films, were characterized by transmission electron microscopy (TEM; 2100F, JEOL, Tokyo, Japan). The photocurrent-voltage characteristics of perovskite solar cells were measured with Keithley 2400 source meter under the simulated AM 1.5G illumination (100mW/cm<sup>2</sup>; Oriol Sol3A Class AAA Solar Simulator, Newport) calibrated with optical power meter (Newport, 1918-R). The I-V curves were obtained through reverse scan (1 V to -0.1 V) with step size of 11 mV and delay time of 20 ms. IPCE spectra were measured by a Newport QE system equipped with a 300 mW xenon light and a lock-in amplifier. All samples for characterization were prepared on the substrates FTO/compact TiO<sub>2</sub>/mesoporous TiO<sub>2</sub> with the same procedure of preparing thin films applied in solar cells, unless stated otherwise.

## Result and discussion

### Buildup of nanoporous PbI<sub>2</sub> films and its mechanism

Fig.1 (a) presents the procedure for preparation of nanoporous PbI<sub>2</sub> film, whose critical step is dropping IPA onto the surface of the as-prepared PbI<sub>2</sub> film. Within seconds after dropping of IPA, the as-spin-coated PbI<sub>2</sub> film turned to dark yellow from pale yellow, indicating the fast formation of PbI<sub>2</sub>. Compared with compact c-PbI<sub>2</sub> film (Fig. 1b) prepared by the conventional method, the resultant PbI<sub>2</sub> film was nanoporous, with pores evenly distributed on the surface of the film, as shown by Fig. 1c. The pore size ranged widely, from 30 nm to 200 nm. To research the distribution of pores inside the n-PbI<sub>2</sub> films, we characterized the cross-section of a planar n-PbI<sub>2</sub> film with ~450 nm in thickness (Fig. 1d and e). Fig. 1d and e show that the n-PbI<sub>2</sub> film is nanoporous throughout the entire thickness, different from c-PbI<sub>2</sub> films reported previously which are totally compact.<sup>35,36</sup> Furthermore, it demonstrates the effectiveness of the SSE method to prepare n-PbI<sub>2</sub> films with thickness up to sub-micrometer.

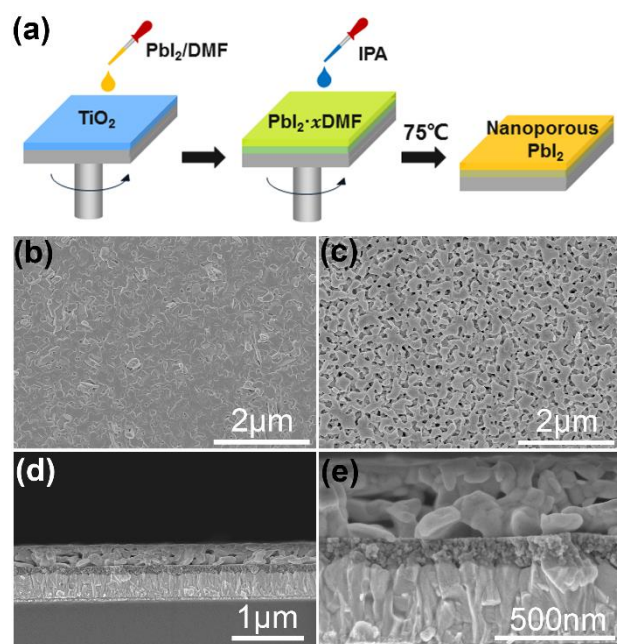
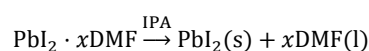


**Fig. 1** (a) Procedure for preparing nanoporous  $\text{PbI}_2$  film.  $\text{PbI}_2$  solution is spin-coated onto the mesoporous  $\text{TiO}_2$  film. Then, the resultant film is dropped with IPA for several seconds before spinning off the remained solvent. Finally, the film is heated at  $75^\circ\text{C}$ . SEM images of (b) c- $\text{PbI}_2$  film prepared with the conventional method and (c) n- $\text{PbI}_2$  film prepared with the SSE method. Cross-sectional SEM images of planar n- $\text{PbI}_2$  film with (d) low magnification and (e) high magnification. The planar n- $\text{PbI}_2$  film was prepared by spin coating 1M  $\text{PbI}_2$  (in DMF) at 2000 r.p.m, followed by SSE process with IPA for 10s.

To gain insight into the preparation mechanism of n- $\text{PbI}_2$  films, XRD spectra were collected in the progression of the SSE process, shown in Fig. 2. Film A was spin-coated from  $\text{PbI}_2$  solution (in DMF), whose colour is pale yellow. Wakamiya *et al.* demonstrated that the pale yellow crystal was  $\text{PbI}_2\cdot\text{DMF}$ , with one DMF molecule coordinated to Pb forming one-dimensional structure along its a-axis.<sup>37</sup> It shows two strong peaks at  $9.02^\circ$  and  $9.56^\circ$  corresponding to (011) and (020) planes of  $\text{PbI}_2\cdot\text{DMF}$ , respectively. That is consistent with other reports, except that the relative intensity of the former peak is higher in our study, as shown in Fig. S1a.<sup>37,38</sup> After the SSE process (without annealing), the resultant dark yellow film (Film B) showed a strong peak at  $12.68^\circ$  corresponding to (001) lattice plane of  $\text{PbI}_2$  (Fig. 2a-red curve), which testifies the crystallization of  $\text{PbI}_2$ . Meanwhile, the peaks of  $\text{PbI}_2\cdot\text{DMF}$  decreased to be negligible, indicating the effective extraction of DMF molecular from  $\text{PbI}_2\cdot\text{DMF}$  by IPA. The extraction of DMF by IPA was confirmed by FTIR characterization as well. As shown in Fig. 2b, the C=O stretching band at  $\sim 1650$  of DMF (shown in Fig. S1c) disappeared, indicating most of DMF is removed. Upon further annealing, the (001) peak of  $\text{PbI}_2$  became sharper, while the peaks corresponding to  $\text{PbI}_2\cdot\text{DMF}$  disappeared completely, resulting in a highly crystallized nanoporous  $\text{PbI}_2$  film. Furthermore, the nanoporous  $\text{PbI}_2$  film showed similar XRD pattern with that from conventional method, indicating that the SSE process would not change the preferential orientation or crystallinity of  $\text{PbI}_2$  film deposited on a mesoporous  $\text{TiO}_2$  layer, as shown in Fig. S1b.

Based on the analyses of XRD and FTIR spectra in the evolution of SSE process, we propose a mechanism

schematically, as shown in Fig. 2c. The main reaction in SSE process is listed as follows:



Here we cautiously use  $x$  ( $x \geq 1$ ) rather than precise stoichiometric ratio, because it is possible that some DMF molecules remain in the film without coordinating to  $\text{PbI}_2$ , as the case of  $\text{PbI}_2\cdot\text{DMSO}$  films.<sup>18</sup> As the reaction equation shows,  $\text{PbI}_2$  precipitates immediately once IPA contacts with  $\text{PbI}_2\cdot\text{DMF}$  film, because the extraction of DMF by IPA will dramatically increase the supersaturation of  $\text{PbI}_2$ . Moreover, the density of  $\text{PbI}_2$  crystal ( $6.1 \text{ g/cm}^3$ ) is much larger than that of  $\text{PbI}_2\cdot\text{DMF}$  ( $3.7 \text{ g/cm}^3$ )<sup>37</sup>, not to speak of the  $\text{PbI}_2\cdot x\text{DMF}$  films. So, the fast transformation from  $\text{PbI}_2\cdot x\text{DMF}$  to  $\text{PbI}_2$  will lead to a shrink in volume (Fig 2c), resulting in many nanopores. As Fig.2c shows, the nanopores formed outside, resulting from the volume shrinkage, facilitates further penetration of the IPA liquids deeper inside the film. Therefore, this solvent extraction reaction can take place thoroughly. As a result, well-structured interpenetrating pores are developed in the entire thickness. This structure is important for the subsequent perovskite conversion reaction. Note that the structure-building process tactfully utilizes the volume shrink effect in the direction from outside to inside rather than the reverse direction as the conventional annealing method does. In conclusion, the  $\text{PbI}_2$  film crystallizes from outside to inside with volume shrink as time goes on before spinning off the solvent, resulting in the interpenetrating nanoporous microstructure throughout the entire thickness.

While the DMF (precursor solvent) /IPA (extraction solvent) combination reported here is just a typical example for preparation of n- $\text{PbI}_2$  films with the SSE method, wide choices of precursor/extraction solvent combination are suitable for it. For example, DMF/toluene combination can be used to prepare n- $\text{PbI}_2$  films, as Fig. S2 shows. Here, we propose some general rules for preparing n- $\text{PbI}_2$  films using the SSE process: (1) The precursor solvents should have high solubility for  $\text{PbI}_2$ . And a high boiling point is preferred, preventing the evaporation-induced crystallization of  $\text{PbI}_2$ ; (2) The extraction solvent should have low solubility for  $\text{PbI}_2$  and relatively low boiling point, in order to dry the films quickly; (3) High intermiscibility between precursor and extraction solvents is necessary, enabling fast SSE process for preparation of n- $\text{PbI}_2$  films.<sup>32</sup>

#### Comparison of c- $\text{PbI}_2$ and n- $\text{PbI}_2$ films for conversion to perovskite

To demonstrate the advantages of nanoporous  $\text{PbI}_2$  films in preparing perovskite films, we carried out absorption test and XRD characterization in the evolution of  $\text{PbI}_2$  conversion into perovskite. As Fig. 3a shows, n- $\text{PbI}_2$  film has a higher absorbance than c- $\text{PbI}_2$ , which may come from the light trapping effect of nanoporous morphology. As a result, the photograph (Fig. S3a) shows n- $\text{PbI}_2$  film is less transparent than c- $\text{PbI}_2$  film. For n- $\text{PbI}_2$  film, the absorbance increases dramatically in the first 10 s when dipped in MAI solution,

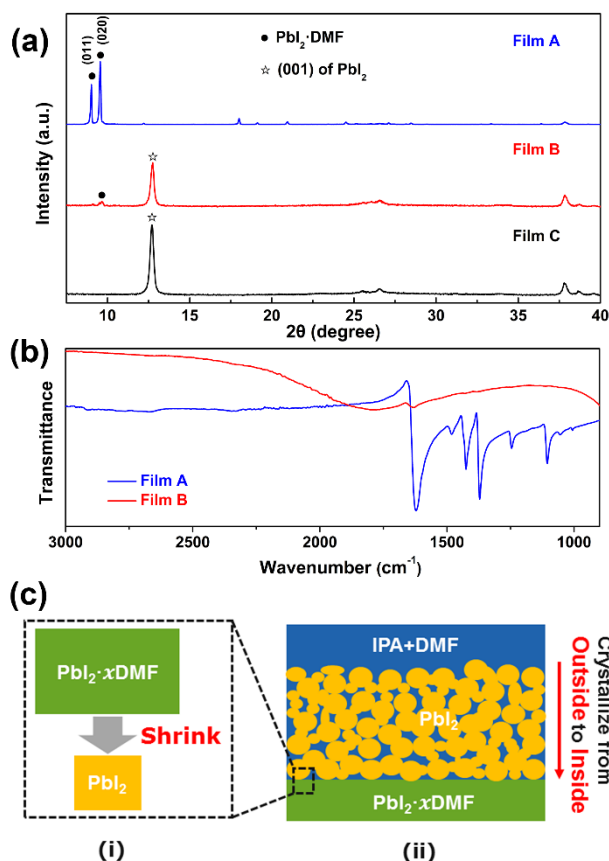


**Fig. 2** (a) XRD and (b) FTIR spectra of as-spun-coated  $\text{PbI}_2$  film without any treatment (Film A), after SSE process for 10 s without annealing (Film B) and with annealing (Film C). The characteristic peaks of  $\text{PbI}_2 \cdot \text{DMF}$  at 9.02 and 9.56 are corresponding to (011) and (020) planes, respectively. (c) Schematic illustration of the SSE process in preparation of nanoporous  $\text{PbI}_2$  films. (i) The volume shrink phenomenon in the transformation from  $\text{PbI}_2 \cdot x\text{DMF}$  to  $\text{PbI}_2$ . (ii) Crystal growth model of n- $\text{PbI}_2$  film. Until spin off the excessive solvent, IPA was penetrating into the nanoporous  $\text{PbI}_2$  frame which had already formed, so  $\text{PbI}_2$  crystallized gradually from outside to inside.

indicating the fast formation of perovskite. That is confirmed by the XRD test, as shown by Fig. 3b, where the (001) peak of  $\text{PbI}_2$  (near  $12.6^\circ$ ) is weak compared with the (110) peak of perovskite (near  $14.1^\circ$ ).<sup>39</sup> As the reaction goes on, the absorbance of the film increases a little (Fig. 3a) and the peaks of  $\text{PbI}_2$  in XRD spectra recede (Fig. 3b). Though trace of  $\text{PbI}_2$  remained after reacting for 90 s, some reports showed that the remnant  $\text{PbI}_2$  would not deteriorate the performance of solar cells.<sup>23,40</sup> While the c- $\text{PbI}_2$  film shows a different conversion behaviour, as shown in Fig. S4. When c- $\text{PbI}_2$  film is dipped into MAI solution for 1 min, the absorbance changes little compared with that of c- $\text{PbI}_2$ , suggesting that the reaction is slow. The slowness of the reaction is also confirmed by XRD characterization. As Fig. S4b shows, the (110) peak of perovskite is extremely weak when dipped for 1 min. Although the intensity of perovskite peak increases with the receding of  $\text{PbI}_2$  peak as dipping time prolongs, there is still a noticeable amount of  $\text{PbI}_2$  remained as indicated by the characteristic  $\text{PbI}_2$  diffraction peak. The  $\text{PbI}_2$  peak disappears until dipping for as long as 30 min. However, dipping too long results in the dissolution of perovskite film, shown by a weaker absorbance as dipping time increases from 10 min to 30 min (Fig. S4a),

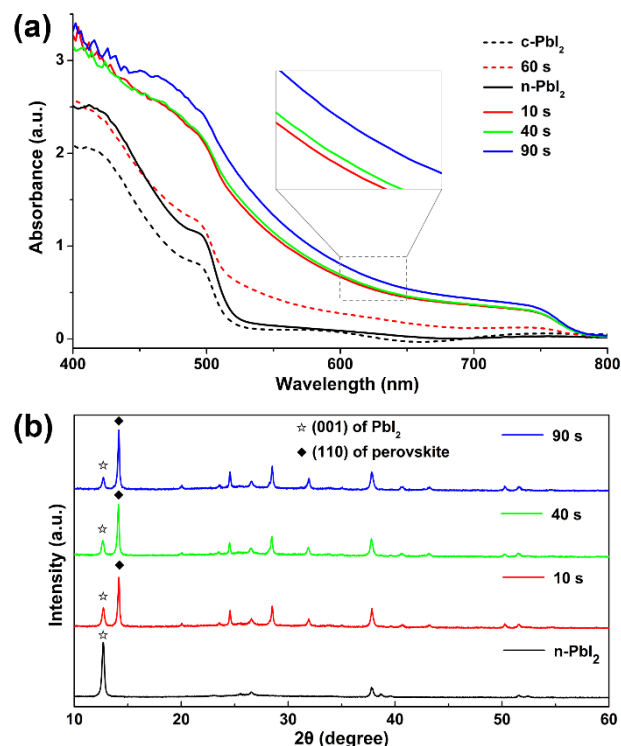


**Fig. 3** Effect of dipping time in MAI solution (10 mg/ml, in IPA) on the evolution of (a) UV-vis absorption spectra and (b) XRD spectra of perovskite films based on c- $\text{PbI}_2$  films (short dash lines) and n- $\text{PbI}_2$  films (solid lines).

reported by Zhao and Zhu as well.<sup>25</sup> Furthermore, prolonging the dipping time will result in the abnormal growth of perovskite crystals, as shown by Fig. S5, enhancing surface recombination as a result of the direct contact between Ag and perovskite layers.<sup>41</sup>

Taking into consideration that the reaction between  $\text{PbI}_2$  and MAI is a solid-liquid reaction, we believe that the reaction rate is determined by three factors: (1) temperature of the reaction system; (2) concentration of MAI solution (keep the solvent as IPA); (3) properties of  $\text{PbI}_2$  films, such as preferential orientation of crystals, crystallinity and morphology of  $\text{PbI}_2$  films. In our study, the first two factors have been carefully controlled. And both of preferential orientation and crystallinity in c- $\text{PbI}_2$  film and n- $\text{PbI}_2$  film shows no difference, as shown in Fig. S1b. So we believe that the great difference between c- $\text{PbI}_2$  and n- $\text{PbI}_2$  films in the preparation of perovskite comes from the morphology difference, as shown in Fig. 4. Mainly, two factors contribute to the faster conversion of n- $\text{PbI}_2$  into perovskite than c- $\text{PbI}_2$ : Firstly, the interpenetrating nanoporous morphology enables the reaction happened in the entire film simultaneously with much more reaction sites, while the reaction is mainly limited to flat surface in the case of c- $\text{PbI}_2$  films; Secondly, both of the particle size and crystallite size are lower in the n- $\text{PbI}_2$  than those of c- $\text{PbI}_2$ , as shown in Fig. 1b, c and Fig. S6, shortening the diffusion length for MAI.<sup>43</sup> In a word, the reaction is limited by the interface of  $\text{PbI}_2$  (s)-MAI (l), so the morphology of  $\text{PbI}_2$  films does matter in the two-step method. Though Ko *et al.* tried to show the importance of  $\text{PbI}_2$  morphology in the two-step method, they failed to exclude the influence



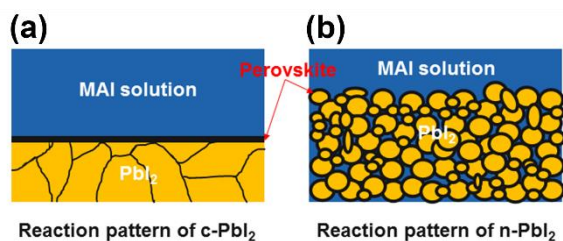


**Fig. 4** Reaction patterns of (a) c-PbI<sub>2</sub> film and (b) n-PbI<sub>2</sub> film in the conversion of PbI<sub>2</sub> into MAPbI<sub>3</sub> perovskite. The c-PbI<sub>2</sub> film consists of large pancake-like layer crystals (200–300 nm), which is so compact that only little MAI solution is able to penetrate into inside through the crystal interfaces.<sup>42</sup> As a result, the reaction is confined to the surface and some interfaces of crystals. Consequently, the reaction is controlled by the diffusion of MAI in the formed perovskite layers.<sup>43</sup> While the n-PbI<sub>2</sub> film is composed of smaller crystals (50–150 nm) with nanoporous morphology, so that MAI is able to penetrate into nanoporous PbI<sub>2</sub> frame once dipped into MAI solution. Therefore, the reaction is going on within the entire film with large surfaces simultaneously. Moreover, the crystals in n-PbI<sub>2</sub> film are much smaller than those in c-PbI<sub>2</sub> film, accelerating the reaction further.

of crystallinity difference of PbI<sub>2</sub>.<sup>44</sup> In this study, however, we succeed to demonstrate the important role of the PbI<sub>2</sub> morphology in the conversion of PbI<sub>2</sub> into perovskite without the interference of crystallinity difference, as shown in Fig. S1b.

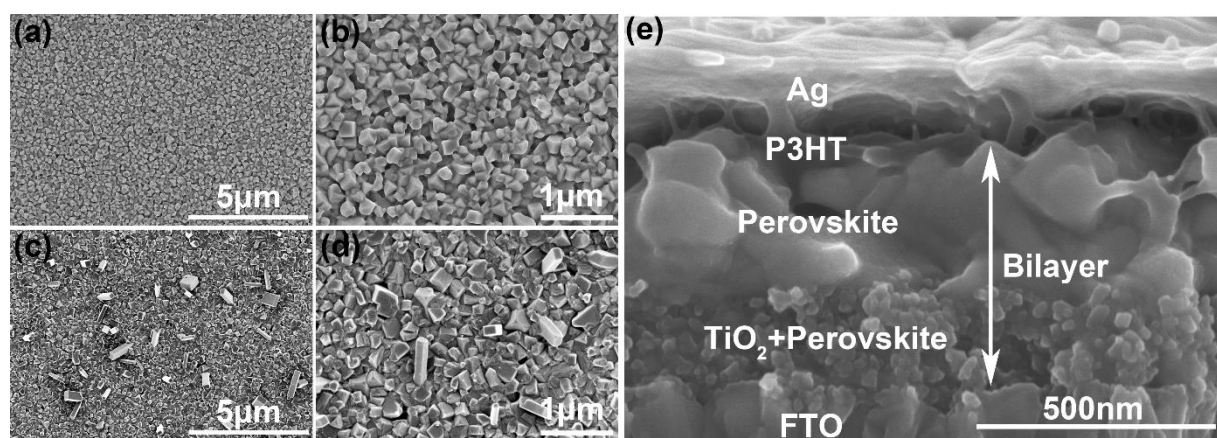
There may be a question about the compactness of the perovskite overlayer in the bilayer-structured solar cells, as n-PbI<sub>2</sub> films are nanoporous. To our surprises, the n-PbI<sub>2</sub> based perovskite overlayer is really compact without any obvious pinholes, as shown in Fig. 5a, b and Fig S7, which can be explained by the volume expansion from the originally edge-sharing octahedral PbI<sub>2</sub> framework (density 6.16 g/cm<sup>3</sup>) to the corner-sharing octahedral structure in perovskite (density 4.16 g/cm<sup>3</sup>).<sup>15,45</sup> Specifically, for 1 mol PbI<sub>2</sub> precursor, its volume evolved from 74.8 cm<sup>3</sup> to 149.0 cm<sup>3</sup> in the conversion of PbI<sub>2</sub> into CH<sub>3</sub>NH<sub>3</sub>PbI<sub>3</sub>, consistent with previous report.<sup>45</sup> The compactness of the perovskite overlayer is testified by the cross-sectional SEM image of a typical perovskite solar cell as well, shown in Fig. 5e. As Fig. 5e shows, a compact perovskite overlayer of 300 nm covers on a 200 nm mesoporous layer, without any pinholes. Contrastively, some micro-size crystals grow on surface of c-PbI<sub>2</sub> based perovskite film when c-PbI<sub>2</sub>

was dipped into MAI solution for 10 min in order to complete the conversion, as shown in Fig. 5c and d. In conclusion, our method manages to fabricate relatively smooth perovskite films without pinholes on the premise that PbI<sub>2</sub> is able to convert into perovskite completely and quickly.

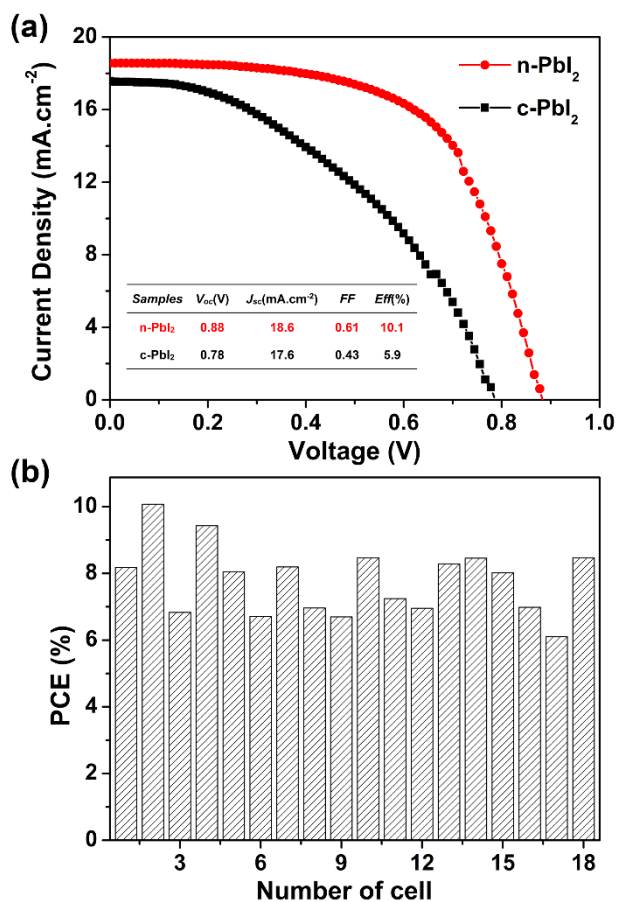
#### Photovoltaic performance of perovskite solar cells

Fig. 6a shows J-V curves of the champion devices with bilayer structure based on n-PbI<sub>2</sub> and c-PbI<sub>2</sub> films, respectively. The solar cell based on n-PbI<sub>2</sub> shows much better performance than that of c-PbI<sub>2</sub>, with V<sub>oc</sub> and J<sub>sc</sub> improved for 0.1 V and 1 mA·cm<sup>-2</sup>, respectively. While the biggest difference lies in the fill factor (FF), which increases from 0.43 to over 0.6 when n-PbI<sub>2</sub> film replaces c-PbI<sub>2</sub> film resulting in a much shorter reaction time in MAI solution.

The improvement of V<sub>oc</sub> and FF mainly came from the suppression of surface recombination, by avoiding the direct contact between Ag and perovskite layers in our case.<sup>41</sup> For n-PbI<sub>2</sub>, 40 s was enough for the conversion, which was too short for the abnormal growth of perovskite crystals, indicated by Fig. 5a and b. As a result, the perovskite can be covered evenly by a thin P3HT layer avoiding the direct contact between Ag and perovskite, indicated by the smooth Ag layer shown in Fig. 5e. On the contrary, c-PbI<sub>2</sub> based perovskite layer became too rough to be completely covered by P3HT layer, when dipped too long for the sake of complete conversion into perovskite (as shown in Fig. S5). Another factor deteriorating the FF in c-PbI<sub>2</sub> based solar cells may come from the reactive Ag electrode. The contacts between Ag and CH<sub>3</sub>NH<sub>3</sub>PbI<sub>3</sub> results in the insulated AgI layer<sup>46</sup>, whose E<sub>VB</sub> (-6.88 eV<sup>47</sup>) is more negative than that of CH<sub>3</sub>NH<sub>3</sub>PbI<sub>3</sub> (-5.43 eV<sup>11</sup>), making it impossible for holes to inject into AgI. As a result, it may cause more severe recombination between electrons and holes in CH<sub>3</sub>NH<sub>3</sub>PbI<sub>3</sub> layer. While that will not happen in the case of Au electrode. Therefore, FF of c-PbI<sub>2</sub> based



**Fig. 5** SEM images of perovskite based on n-PbI<sub>2</sub> film (a), (b) and based on c-PbI<sub>2</sub> film (c), (d). Perovskite films were prepared by dipping n-PbI<sub>2</sub> and c-PbI<sub>2</sub> films into MAI solution (10 mg/ml, in IPA) for 40 s and 10 min, respectively. (e) Cross-sectional SEM image of perovskite solar cell with bilayer structure. The perovskite overlayer is compact without any obvious pinholes, whose thickness is ~300 nm.



**Fig. 6** (a) The best photovoltaic performance of devices based on n-PbI<sub>2</sub> and c-PbI<sub>2</sub> films, which are dipped in MAI solution for 40 s and 10 min, respectively. Both of the dipping time were determined to be optimal in the preliminary tests. (b) Histogram of power conversion efficiency of perovskite films based on n-PbI<sub>2</sub> films.

solar cell, even with a thin layer of P3HT, is much lower than that of HTM-free case with Au as back electrode.<sup>41</sup> Those reasons mentioned above contribute to the slight rise in J<sub>sc</sub> of n-PbI<sub>2</sub> based solar cell as well, apart from the enhanced absorption of perovskite layer resulting from the reflection of smooth Ag layer.<sup>41</sup> As a consequence, the efficiency almost doubled with n-PbI<sub>2</sub> method, rising from 5.9% to 10.1%. Furthermore, Fig. 6b gives the histogram plots of PCE (solar cells based on n-PbI<sub>2</sub>), showing the average PCE is ~ 8%. More information about V<sub>oc</sub> and J<sub>sc</sub> statistics are shown in Fig. S8, demonstrating their average at 17 mA·cm<sup>-2</sup> and 0.85 V, respectively. IPCE spectra of perovskite solar cells with medium performance are shown in Fig. S9, and the measured J<sub>sc</sub> from the J-V curves agree well with the integrated J<sub>sc</sub> from

IPCE spectra. Further improvement of device performance may lie in the optimization of hole transport layers, such as replacing P3HT with Spiro-MeOTAD.<sup>48</sup> The nanoporous PbI<sub>2</sub> assisted two-step method accelerates the conversion of PbI<sub>2</sub> into perovskite significantly compared to conventional method, and the resultant perovskite films are comparatively compact. Therefore, this method can be applied to prepare phase-pure compact planar perovskite films in short time, overcoming the disadvantages of the conventional two-step method. Moreover, this method is promising to fabricate perovskite films with interpenetrating nanopores by controlling the porosity and pore size of PbI<sub>2</sub>. And that will lead to realizing a new kind of perovskite solar cells with porous perovskite p-n heterojunction, in which porous perovskite layer is infiltrated with transparent charge transport material.<sup>49</sup>

## Conclusion

We have demonstrated a facile way to prepare nanoporous PbI<sub>2</sub> films with the SSE method, which effectively accelerates the reaction between PbI<sub>2</sub> and MAI. Insights into the mechanism of preparing nanoporous PbI<sub>2</sub> films with the SSE method are provided, suggesting that the nanoporous morphology of PbI<sub>2</sub> comes from the synergic effect of volume shrink effect and fast crystallization from outside to inside. Using this method, we are able to prepare well-crystallized nanoporous PbI<sub>2</sub> films within seconds without annealing. Furthermore, we applied the nanoporous PbI<sub>2</sub> to preparing perovskite films, showing that most part of PbI<sub>2</sub> has converted into perovskite within 10 s. Based on this, an interface-limited reaction model is proposed in the reaction system of PbI<sub>2</sub> (s)-MAI (l). Moreover, a pinhole-free perovskite overlayer is obtained, due to the volume expansion effect in the conversion of PbI<sub>2</sub> into perovskite. As a result, a champion PCE over 10% has been achieved. This study uncovers the PbI<sub>2</sub>-morphology-related kinetics in the two-step deposition method, and may open up a promising avenue for preparing high quality perovskite films by controlling the properties of PbI<sub>2</sub> films.

## Acknowledgement

This work was supported by the National Basic Research Program of China (2012CB932303), the National Natural Science Foundation of China (Grant No. 51272265, 61574148) and the Leading Youth Talent Project of Jiading District (2013).

## Notes and references

- S. De Wolf, J. Holovsky, S. Moon, P. Löper, B. Niesen, M. Ledinsky, F. Haug, J. Yum and C. Ballif, *J. Phys. Chem. Lett.*, 2014, **5**, 1035-1039.
- S. D. Stranks, G. E. Eperon, G. Grancini, C. Menelaou, M. J. P. Alcocer, T. Leijtens, L. M. Herz, A. Petrozza and H. J. Snaith, *Science*, 2013, **342**, 341-344.
- G. Xing, N. Mathews, S. Sun, S. S. Lim, Y. M. Lam, M. Gratzel, S. Mhaisalkar and T. C. Sum, *Science*, 2013, **342**, 344-347.
- D. Shi, V. Adinolfi, R. Comin, M. Yuan, E. Alarousu, A. Buin, Y. Chen, S. Hoogland, A. Rothenberger, K. Katsiev, Y. Losovyj, X. Zhang, P. A. Dowben, O. F. Mohammed, E. H. Sargent and O. M. Bakr, *Science*, 2015, **347**, 519-522.
- G. E. Eperon, S. D. Stranks, C. Menelaou, M. B. Johnston, L. M. Herz and H. J. Snaith, *Energy Environ. Sci.*, 2014, **7**, 982-988.
- Y. Ogomi, A. Morita, S. Tsukamoto, T. Saitho, N. Fujikawa, Q. Shen, T. Toyoda, K. Yoshino, S. S. Pandey, T. Ma and S. Hayase, *J. Phys. Chem. Lett.*, 2014, **5**, 1004-1011.
- N. Pellet, P. Gao, G. Gregori, T. Yang, M. K. Nazeeruddin, J. Maier and M. Grätzel, *Angew. Chem., Int. Ed.*, 2014, **53**, 3151-3157.
- J. H. Noh, S. H. Im, J. H. Heo, T. N. Mandal and S. I. Seok, *Nano Lett.*, 2013, **13**, 1764-1769.
- S. A. Kulkarni, T. Baikie, P. P. Boix, N. Yantara, N. Mathews and S. Mhaisalkar, *J. Mater. Chem. A*, 2014, **2**, 9221-9225.
- W. S. Yang, J. H. Noh, N. J. Jeon, Y. C. Kim, S. Ryu, J. Seo and S. I. Seok, *Science*, 2015, **348**, 1234-1237.
- H. Kim, C. Lee, J. Im, K. Lee, T. Moehl, A. Marchioro, S. Moon, R. Humphry-Baker, J. Yum, J. E. Moser, M. Graetzel and N. Park, *Sci. Rep.*, 2012, **2**, 591.
- M. M. Lee, J. Teuscher, T. Miyasaka, T. N. Murakami and H. J. Snaith, *Science*, 2012, **338**, 643-647.
- J. Burschka, N. Pellet, S. Moon, R. Humphry-Baker, P. Gao, M. K. Nazeeruddin and M. Grätzel, *Nature*, 2013, **499**, 316-319.
- M. Liu, M. B. Johnston and H. J. Snaith, *Nature*, 2013, **501**, 395-398.
- Q. Chen, H. Zhou, Z. Hong, S. Luo, H. Duan, H. Wang, Y. Liu, G. Li and Y. Yang, *J. Am. Chem. Soc.*, 2014, **136**, 622-625.
- J. Im, H. Kim and N. Park, *APL Mater.*, 2014, **2**, 081510.
- N. Yantara, D. Sabba, F. Yanan, J. M. Kadro, T. Moehl, P. P. Boix, S. Mhaisalkar, M. Gratzel and C. Gratzel, *Chem. Commun.*, 2015, **51**, 4603-4606.
- Y. Wu, A. Islam, X. Yang, C. Qin, J. Liu, K. Zhang, W. Peng and L. Han, *Energy Environ. Sci.*, 2014, **7**, 2934-2938.
- N. J. Jeon, J. H. Noh, Y. C. Kim, W. S. Yang, S. Ryu and S. Il Seol, *Nat. Mater.*, 2014, **13**, 897-903.
- G. Li, K. L. Ching, J. Y. L. Ho, M. Wong and H. Kwok, *Adv. Energy Mater.*, 2015, **5**, 1401775.
- J. Shi, Y. Luo, H. Wei, J. Luo, J. Dong, S. Lv, J. Xiao, Y. Xu, L. Zhu, X. Xu, H. Wu, D. Li and Q. Meng, *ACS Appl. Mater. Interfaces*, 2014, **6**, 9711-9718.
- Y. Xie, F. Shao, Y. Wang, T. Xu, D. Wang and F. Huang, *ACS Appl. Mater. Interfaces*, 2015, **7**, 12937-12942.
- D. H. Cao, C. C. Stoumpos, C. D. Malliakas, M. J. Katz, O. K. Farha, J. T. Hupp and M. G. Kanatzidis, *APL Mater.*, 2014, **2**, 091101.
- B. E. Cohen, S. Gamliel and L. Etgara, *APL Mater.*, 2014, **2**, 081502.
- Y. Zhao and K. Zhu, *J. Mater. Chem. A*, 2015, **3**, 9086-9091.
- L. Zheng, Y. Ma, S. Chu, S. Wang, B. Qu, L. Xiao, Z. Chen, Q. Gong, Z. Wu and X. Hou, *Nanoscale*, 2014, **6**, 8171-8176.
- P. Docampo, F. C. Hanusch, S. D. Stranks, M. Doeblinger, J. M. Feckl, M. Ehrensperger, N. K. Minar, M. B. Johnston, H. J. Snaith and T. Bein, *Adv. Energy Mater.*, 2014, **4**, 1400355.
- J. Xi, Z. Wu, H. Dong, B. Xia, F. Yuan, B. Jiao, L. Xiao, Q. Gong and X. Hou, *Nanoscale*, 2015, **7**, 10699-10707.
- F. Fu, L. Kranz, S. Yoon, J. Löckinger, T. Jäger, J. Perrenoud, T. Feurer, C. Gretener, S. Bücheler and A. N. Tiwari, *Phys. Status Solidi A*, 2015, DOI: 10.1002/pssa.201532442.
- C. Ying, C. Shi, N. Wu, J. Zhang and M. Wang, *Nanoscale*, 2015, **7**, 12092-12095.
- Y. Zhou, M. Yang, A. L. Vasiliev, H. F. Garces, Y. Zhao, D. Wang, S. Pang, K. Zhu and N. P. Padture, *J. Mater. Chem. A*, 2015, **3**, 9249-9256.
- Y. Zhou, M. Yang, W. Wu, A. L. Vasiliev, K. Zhu and N. P. Padture, *J. Mater. Chem. A*, 2015, **3**, 8178-8184.
- P. Docampo, J. M. Ball, M. Darwich, G. E. Eperon and H. J. Snaith, *Nat. Commun.*, 2013, **4**, 2761.
- J. H. Heo and S. H. Im, *Phys. Status Solidi RRL*, 2014, **8**, 816-821.
- T. Du, N. Wang, H. Chen, H. Lin and H. He, *ACS Appl. Mater. Interfaces*, 2015, **7**, 3382-3388.
- Z. Xiao, C. Bi, Y. Shao, Q. Dong, Q. Wang, Y. Yuan, C. Wang, Y. Gao and J. Huang, *Energy Environ. Sci.*, 2014, **7**, 2619-2623.
- A. Wakamiya, M. Endo, T. Sasamori, N. Tokitoh, Y. Ogomi, S. Hayase and Y. Murata, *Chem. Lett.*, 2014, **43**, 711-713.
- D. Shen, X. Yu, X. Cai, M. Peng, Y. Ma, X. Su, L. Xiao and D. Zou, *J. Mater. Chem. A*, 2014, **2**, 20454-20461.
- T. Baikie, Y. Fang, J. M. Kadro, M. Schreyer, F. Wei, S. G. Mhaisalkar, M. Graetzel and T. J. White, *J. Mater. Chem. A*, 2013, **1**, 5628-5641.
- Q. Chen, H. Zhou, T. Song, S. Luo, Z. Hong, H. Duan, L. Dou, Y. Liu and Y. Yang, *Nano Lett.*, 2014, **14**, 4158-4163.
- N. Marinova, W. Tress, R. Humphry-Baker, M. I. Dar, V. Bojinov, S. M. Zakeeruddin, M. K. Nazeeruddin and M. Grätzel, *ACS Nano*, 2015, **9**, 4200-4209.
- J. Schlipf, P. Docampo, C. J. Schaffer, V. Körstgens, L. Bießmann, F. Hanusch, N. Giesbrecht, S. Bernstorff, T. Bein and P. Müller-Buschbaum, *J. Phys. Chem. Lett.*, 2015, 1265-1269.
- Y. Zhao and K. Zhu, *J. Phys. Chem. Lett.*, 2014, **5**, 4175-4186.
- H. Ko, J. Lee and N. Park, *J. Mater. Chem. A*, 2015, **3**, 8808-8815.
- D. Liu, M. K. Gangishetty and T. L. Kelly, *J. Mater. Chem. A*, 2014, **2**, 19873-19881.
- Y. Han, S. Meyer, Y. Dkhissi, K. Weber, J. M. Pringle, U. Bach, L. Spiccia and Y. Cheng, *J. Mater. Chem. A*, 2015, **3**, 8139-8147.
- B. Chen, Y. Deng, H. Tong and J. Ma, *Superlattices Microstruct.*, 2014, **69**, 194-203.
- D. Bi, L. Yang, G. Boschloo, A. Hagfeldt and E. M. J. Johansson, *J. Phys. Chem. Lett.*, 2013, **4**, 1532-1536.
- H. J. Snaith, *J. Phys. Chem. Lett.*, 2013, **4**, 3623-3630.